AN OVERVIEW OF COMPUTATIONAL AEROACOUSTIC MODELING AT NASA LANGLEY

DAVID P. LOCKARD
Aerodynamics, Aerothermodynamics, and Acoustics Competency
NASA Langley Research Center
Hampton, VA 23681-2199, U.S.A

ABSTRACT

The use of computational techniques in the area of acoustics is known as computational aeroacoustics and has shown great promise in recent years. Although an ultimate goal is to use computational simulations as a virtual wind tunnel, the problem is so complex that blind applications of traditional algorithms are typically unable to produce acceptable results. The phenomena of interest are inherently unsteady and cover a wide range of frequencies and amplitudes. Nonetheless, with appropriate simplifications and special care to resolve specific phenomena, currently available methods can be used to solve important acoustic problems. These simulations can be used to complement experiments, and often give much more detailed information than can be obtained in a wind tunnel. The use of acoustic analogy methods to inexpensively determine far-field acoustics from near-field unsteadiness has greatly reduced the computational requirements. A few examples of current applications of computational aeroacoustics at NASA Langley are given. There remains a large class of problems that require more accurate and efficient methods. Research to develop more advanced methods that are able to handle the geometric complexity of realistic problems using block-structured and unstructured grids are highlighted.

INTRODUCTION

Computational aeroacoustics is a very broad field that encompasses research that uses numerical simulations to better understand aerodynamic noise. There is a large computational effort at NASA Langley Research Center aimed at predicting and reducing aircraft noise, and this paper only attempts to give an overview of a representative fraction of that work. The problem is very difficult because the geometry and physics involved are often quite complex. It has taken 30 years to achieve significant noise reduction for jet engines. Although great strides have been made in the reduction of jet noise through the use of high-bypass ratio engines, there is a lack of understanding of the fundamental noise sources in subsonic jets. Today, tonal noise from large inlet fans is also important. There is a general theory for fan noise, but calculations are still somewhat limited. Extensive research is ongoing in the areas of duct and liner acoustics[1]. Furthermore, the engines are not the only noise source that must be considered. Reductions in jet noise have made the airframe a significant, and in some cases dominant source during landing. The flaps, slats, and landing gear are all important contributors to the sound field. To achieve significant noise reduction, these three major landing systems and the engines must all be quieted commensurately.

The physics behind the unsteadiness that generates noise is also very complicated. Fluctuations tend to grow in shear layers and vortical structures. Resolving these features in a mean flow calculation can be difficult. Trying to capture the unsteadiness growing in them is even more challenging. Separated regions, instabilities, and large and small scale turbulence structures can all contribute to the sound field. Furthermore, the energy that is radiated as noise is typically only a small fraction of the total energy near the source. This is part of the scale disparity between acoustic and hydrodynamic fluctuations. The human ear is able to distinguish between signals with vastly varying amplitudes, so it is typical to use a logarithmic scale to describe them. The sound pressure level (SPL) is given by

$$\mathrm{SPL} = 20\ \log(\frac{p'_{rms}}{p_{ref}}) \tag{1}$$

with units of decibels (dB). The reference pressure $p_{ref} = 20 \times 10^{-6}$ Pa is the threshold of human hearing, and rms means root mean square. The ratio of pressure amplitudes between a quiet conversation, 60 dB, and a rock concert, 120 dB, is 1000. In addition, atmospheric pressure is 3500 times greater than the pressure amplitude of a 120 dB signal. At 120 dB, one starts feeling discomfort and experiences a ringing in the ears. Although this level is very loud

to humans, it is so small that a typical computational fluid dynamics (CFD) simulation very easily loses the sound waves among the large hydrodynamic fluctuations. Simultaneously resolving the hydrodynamic fluctuations and the wide range of acoustic signals is very difficult.

Acousticians also have to deal with very disparate length and time scales. Mostly people can hear fairly well between frequencies of 100 Hz and 10 kHz. This corresponds to wavelengths of 0.11 ft (0.034 m) and 11 ft (3.4 m), respectively. Trying to have enough grid points in the domain to resolve the very short wavelength while having a domain large enough to encompass the long wavelength results in enormous grids. One is also faced with the challenge of trying to propagate the signal to observers located at great distances from the sources. A similar scale problem occurs temporally. The wavelength λ of an acoustic wave is related to the temporal period T by $\lambda = cT$ where c is the speed of sound. The periods for 100 Hz and 10 kHz are 0.0001 s and 0.01 s, respectively. Hence, one needs many time steps for the short period, and long run times to get a significant sample of the long period. This problem is usually exacerbated by initial transients in numerical solutions which must decay sufficiently before one can start sampling the acoustics. Even when using sampling techniques developed for experimental work, it is difficult to run codes long enough to get statistically significant samples of pseudo-random phenomena. Furthermore, the disparity between different acoustic waves is only part of the problem. One also has to compare the acoustic scales with those of other fluid phenomena and the geometry.

Faced with these challenges, one must inevitably make simplifying assumptions. However, computational methods are often able to relax those used in the past. The basic goal is to obtain an understanding of the underlying physics of the noise sources. One needs to know the strength, location, frequency, wavelength, and nature of the disturbances. With this information one can develop prediction methods that are general across different configurations that have similar source mechanisms generating the noise. Furthermore, one can begin attacking the sources in systematic ways that are more likely to lead to significant noise reduction. To get at the physics, we are using currently available tools and developing new ones to do bigger problems in the future. To reduce the complexity, most calculations concentrate on a small frequency range rather than trying to resolve all of the relevant frequencies at once. In addition, one can solve equations linearized about the mean flow[2, 3] to separate out the acoustic and hydrodynamic scales. Using these simplifications makes many problems tractable to modern methods. Furthermore, numerical applications of acoustic analogy methods have matured significantly, and they allow far-field acoustics to be calculated from unsteady fluctuations in the vicinity of the sources. This greatly reduces the computational effort and provides a means of finding the noise where the observers are actually located.

The remainder of the paper discusses some of the acoustic problems that have been solved using combinations of available methods. First, the CFD code CFL3D is described. It was used in many of the example computations. The acoustic analogy is explained in slightly more detail because it is key to most of the calculations and is less widely known. At the end of the paper, examples of several new technologies under development are discussed. These include high-order methods for block-structured and unstructured grids. Because of the great scale disparities in acoustics, one either needs high-accuracy methods that resolve waves with a minimal number of points-per-wavelength or standard methods with fine grids. Such comparisons[4, 5] have shown that high-order methods are more efficient at resolving acoustic phenomena than traditional methods with extremely fine grids. However, high-order methods often suffer from robustness problems for realistic configurations, and these new efforts are aimed at overcoming this difficulty.

COMPUTATIONAL TOOLS

THE COMPUTER CODE CFL3D

The computer code CFL3D [6, 7] is a robust, workhorse code used to compute both steady and unsteady flow fields. The CFL3D code was developed at NASA Langley Research Center to solve the three-dimensional, time-dependent, thin-layer (in each coordinate direction) Reynolds-averaged Navier-Stokes (RANS) equations using a finite-volume formulation. The code uses upwind-biased spatial differencing for the inviscid terms and flux limiting to obtain smooth solutions in the vicinity of shock waves. The viscous derivatives, when used, are computed by second order central differencing. Fluxes at the cell faces are calculated by flux-difference-splitting. An implicit three-factor approximate factorization method is used to advance the solution in time. Patched grid interfaces, overset grids, and slides zones are available for use at zone boundaries.

The time-dependent version of CFL3D uses subiterations to obtain second order temporal accuracy. In the $\tau - TS$ subiteration option [8], each of the subiterations is advanced with a pseudo-time step. This approach facilitates a

more rapid convergence to the result at each physical time step. The steady-state version of the code employs full multigrid acceleration.

ACOUSTIC ANALOGY

An acoustic analogy is a rearrangement of the governing equations of fluid motion such that the left-hand side consists of a wave operator in an undisturbed medium, and the right-hand side is comprised of acoustic source terms. The solution to the equation can be written as the convolution of the source terms with the Green function for the wave operator. Hence, if one can obtain the strengths of the source terms in the regions where they are significant, one can determine the acoustic signal at any point in the flow, including locations at long distances from the sources. Lighthill[9] was the first to propose this approach. Although this concept is relatively simple, extensive manipulations have been required to put the equations in the most useful forms for analytic and numerical applications.

The Ffowcs Williams and Hawkings [10] equation is the most general form of the Lighthill acoustic analogy and when provided with input of unsteady flow conditions, is appropriate for numerically computing the acoustic field. The equation is derived directly from the equations of conservation of mass and momentum. Following Brentner and Farassat [11], the FW-H equation may be written in differential form as

$$\Box^2 c^2 \rho'(\mathbf{x},t) = \frac{\partial^2}{\partial x_i \partial x_j}[T_{ij}H(f)] - \frac{\partial}{\partial x_i}[L_i \delta(f)] + \frac{\partial}{\partial t}[Q\delta(f)] \tag{2}$$

where: $\Box^2 \equiv \frac{1}{c^2}\frac{\partial^2}{\partial t^2} - \nabla^2$ is the wave operator, c is the ambient speed of sound, t is observer time, ρ' is the perturbation density, ρ_0 is the ambient density, $f = 0$ describes the integration surface, $f < 0$ being inside the integration surface, $\delta(f)$ is the Dirac delta function, and $H(f)$ is the Heaviside function. The quantities Q, U_i and L_i are defined by

$$Q = (\rho_0 U_n), \;\; U_i = (1 - \frac{\rho}{\rho_0})v_i + \frac{\rho u_i}{\rho_0} \;\text{ and }\; L_i = P_{ij}\hat{n}_j + \rho u_i(u_n - v_n)\;. \tag{3}$$

In the above equations, ρ is the total density, ρu_i, is the fluid momentum, v_i is the velocity of the integration surface $f = 0$, and P_{ij} is the compressive stress tensor. For an inviscid fluid, $P_{ij} = p'\delta_{ij}$ where p' is the perturbation pressure and δ_{ij} is the Kronecker delta. The Lighthill stress tensor is given by T_{ij}. The subscript n indicates the component of velocity in the direction normal to the surface.

An integral solution to the FW-H equation (2) can be written in terms of the acoustic pressure $p' = c^2\rho'$ in the region $f > 0$. Utilizing formulation 1A of Farassat [12, 13], the integral representation has the form

$$p'(\mathbf{x},t) = p'_T(\mathbf{x},t) + p'_L(\mathbf{x},t) + p'_Q(\mathbf{x},t) \tag{4}$$

where

$$4\pi p'_Q(\mathbf{x},t) = \int_{f=0} \left[P_Q(\mathbf{y},\tau)\right]_{\text{ret}} dS, \;\; 4\pi p'_L(\mathbf{x},t) = \int_{f=0} \left[P_L(\mathbf{y},\tau)\right]_{\text{ret}} dS. \text{and} \tag{5}$$

$$4\pi p'_T(\mathbf{x},t) = \int_{f=0} \left[P_T(\mathbf{y},\tau)\right]_{\text{ret}} dV. \tag{6}$$

The subscript ret means that the quantities must be evaluated at the appropriate retarded or emission time τ. The kernel functions $P_T,\; P_L,\; P_Q$ are combinations of flow quantities and geometric parameters. For many numerical simulations it is desirable to let the integration surface be permeable and place it within the flow. However, when the surface coincides with a solid body, the terms take on simple meanings. The Q term is known as the thickness contribution and represents the noise generated by the unsteady displacement of fluid by the body. The L term involves the noise caused by the fluctuating loading on the body. The term p'_T accounts for all quadrupoles outside of the integration surface (i.e., $f > 0$). Quadrupole contributions include nonlinear effects and refraction. In most work, p'_T is small and can be neglected. This is important because the quadrupole term involves a volume integration, whereas p'_Q and p'_L only require an integration over the surface. All quadrupole contributions that are within the surface are accounted for by the surface integrations. Hence, the far-field pressure at any instance in time can usually be calculated by integrating the near-field flow quantities over a surface. This allows for very rapid calculations of noise a great distance away from the source region where the integration surface is typically placed.

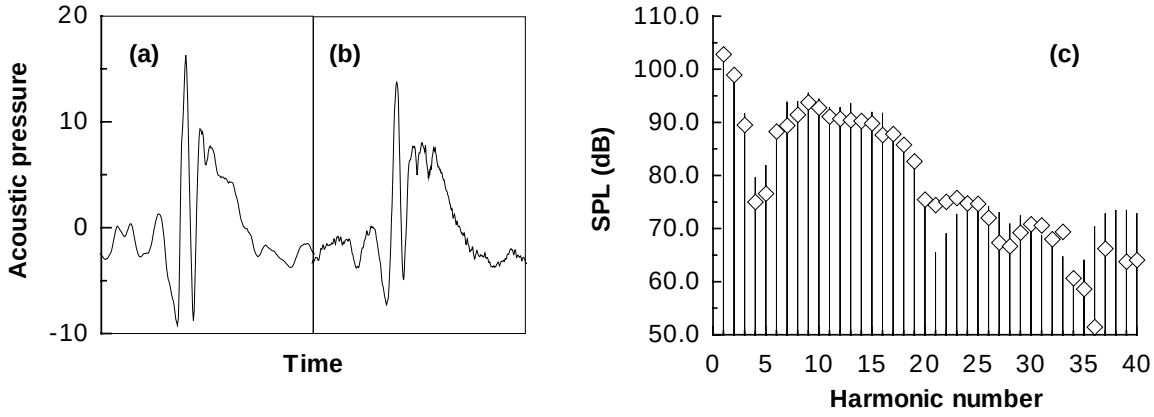

Figure 1. Comparison of measure and computed noise for a four-bladed Sikorsky model rotor. The microphone locations was nominally 25 deg. below the rotor plane on the advancing side, 1.5 rotor radii from the rotor hub. This is a descent condition. (a) Measure time history; (b) predicted time history; (c) spectral comparison (——— measured; ◇ predicted)

Rotorcraft acoustics is an area where the FW-H equation has been utilized with great success. The code WOPWOP[13] has been used extensively by industry and researchers to predict helicopter noise. Even for complex phenomena such as blade vortex interaction (BVI), WOPWOP correctly predicts the acoustic signature when it is given accurate pressure data as inputs. As an example, figure 1 compares the experimentally observed and computed acoustic signals[14] when experimentally measured surface pressures from a four bladed rotor where used as input to WOPWOP. The spectral comparison in figure 1 shows the agreement is good up to the 32nd harmonic. Similar comparisons using CFD data as input do not yield such good results. This underscores the importance of having accurate input data on the integration surface. The acoustic theory is mature enough for such complicated problems, but more accurate CFD is needed.

SAMPLE APPLICATIONS

Although there are many problems that cannot be solved with conventional methods, appropriate assumptions can make many realistic problems tractable. This section provides several examples where current methods were successfully used to simulate important acoustic phenomena.

ROTOR NOISE

Rumsey *et al.*[15] used the Navier-Stokes code CFL3D to predict one of the ducted-fan engine acoustic modes that results from a rotor-wake/stator-blade interaction. A patched-sliding-zone interface was employed to pass information between the moving rotor-row and the stationary stator row. Figure 2 shows the geometry and 2.7 million point grid used in the calculation. The code produced averaged aerodynamic results downstream of the rotor that are in good agreement with a widely used average-passage code. The calculation was designed to capture a single acoustic mode, and the code successfully generated and propagated that mode upstream with minimal attenuation into a region of nearly uniform flow as shown in figure 3(a). Two acoustic codes were used to find the far-field noise. Propagation in the duct was computed by Eversmann's wave envelope code, which is based on a finite-element model. Propagation to the far field was accomplished by using the Kirchhoff formula for moving surfaces. The Kirchhoff method is used in a similar fashion to acoustic analogy methods, but is less general. Comparison of measured and computed far-field noise levels are in fair agreement in the range of directivity angles (20-40 deg.) where the peak radiation lobes are observed for the mode under investigation. Figure 3 compares the experimental and computed results. Although only a single acoustic mode was targeted in this study, it provided a proof of concept: Navier-Stokes codes can be used to both generate and propagate rotor-stator acoustic modes through and engine, where the results can be coupled to other far-field noise prediction codes.

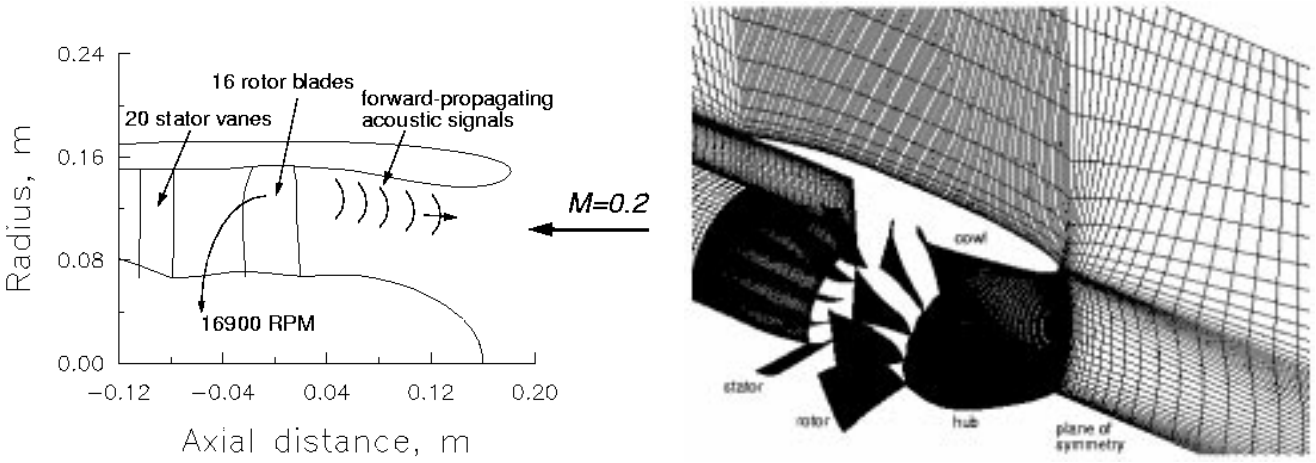

(a) Geometry. (b) 2.7 million point grid.

Figure 2. Geometry and grid for rotor-wake/stator-blade interaction problem.

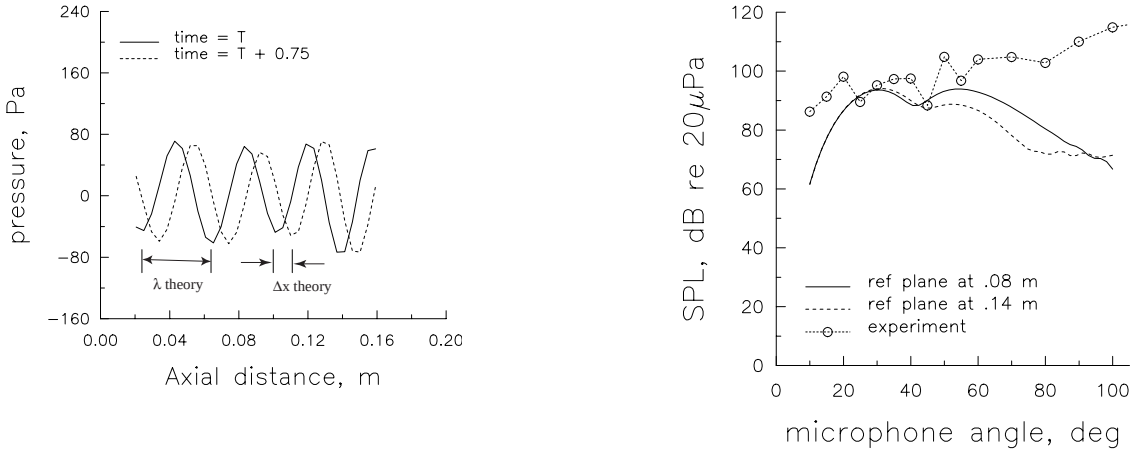

(a) Near-field pressure. (b) Far-field noise.

Figure 3. Near-field pressure computed by CFL3D and far-field pressure computed by Eversmann's wave envelope code and a Kirchhoff technique.

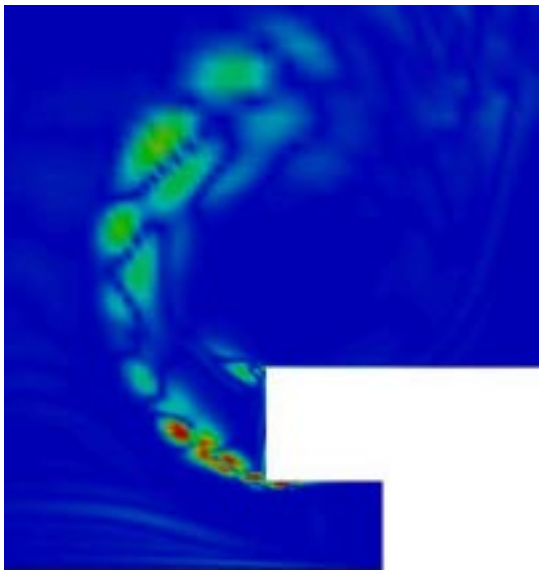

(a) Vorticity Contours

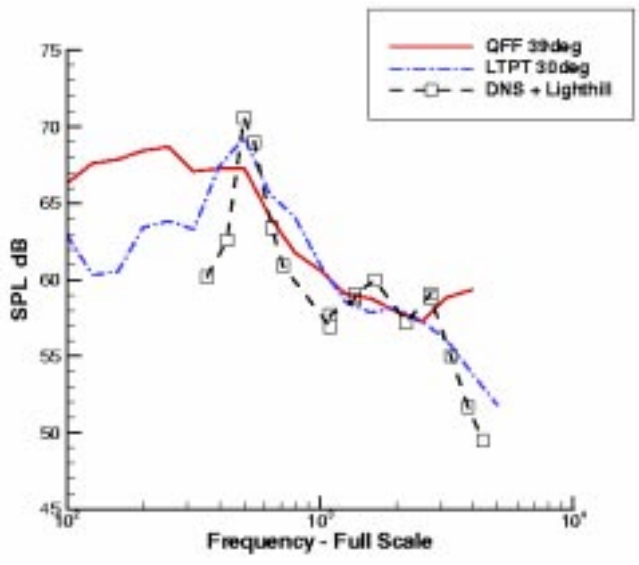

(b) Spectra

Figure 4. (a) Vorticity contours from 2-D DNS of flap-edge flow (b) Comparison of computed and experimental spectra.

FLAP-EDGE NOISE

A different computational framework was developed to simulate the unsteadiness associated with the vortex system around the flap of a high-lift system. The vortex system is surprisingly complex, and a steady RANS calculation with sufficient resolution required 50 CRAY C-90 hours. Clearly, some approximations must be made to deal with the unsteady problem because a DNS would be intractable. Streett[16] simplified the problem by performing a 2-D, incompressible DNS linearized about the RANS mean flow. Because the vortex system varies relatively slowly in the streamwise direction, the DNS calculations were performed at several streamwise stations assuming locally parallel flow. Calculations were performed in a parameter space that included the frequency and a spanwise wavenumber. Figure 4(a) shows the vorticity contours for a case where the spanwise wavenumber was zero, and instabilities dominate in the shear layer formed on the under side of the flap. This instability was persistent from 5 to 30 kHz. For nonzero wavenumbers, an instability within the vortex on top of the flap grew rapidly. Although the DNS simulations show local unsteadiness, they do not reveal how much of that energy propagates to the far-field. The Lighthill acoustic analogy[9] was used for this purpose. This type of formulation allows the source strengths to be computed from incompressible flow because all of the acoustic propagation is taken into account by the analogy. However, the complex geometry in this problem required a numerical solution of the partial differential equation form of the acoustic analogy. The results of those calculations are compared with those from two experiments in figure 4(b). The comparison is quite good, and gives confidence that the instabilities identified by the DNS are indeed generating noise. With the detailed information about the frequencies, wavelengths, and locations of the instabilities from the DNS, techniques to reduce the noise at the source have been developed.

CYLINDER SHEDDING

To determine the sensitivity of the FW-H method to the integration surface location when it passes through a wake, Singer *et al.*[17] examined a circular cylinder in a cross flow. Equivalent calculations were also performed using a Kirchhoff technique. This was important because the shed vortices produce large, unsteady fluctuations as they pass through the surfaces. These fluctuations would be balanced by the quadrupole term in the FW-H if it were included, but it is much more desirable to avoid the volume integration. Furthermore, the Kirchhoff equation is derived from the acoustic wave equation and is strictly valid only in the region of the flow where the wave equation is the appropriate governing equation. This problem tested whether the Kirchoff method can be used with near-field data that includes nonlinear, non-acoustic fluctuations.

Figure 5 renders an instantaneous vorticity field obtained from a CFL3D calculation with a superimposed grid

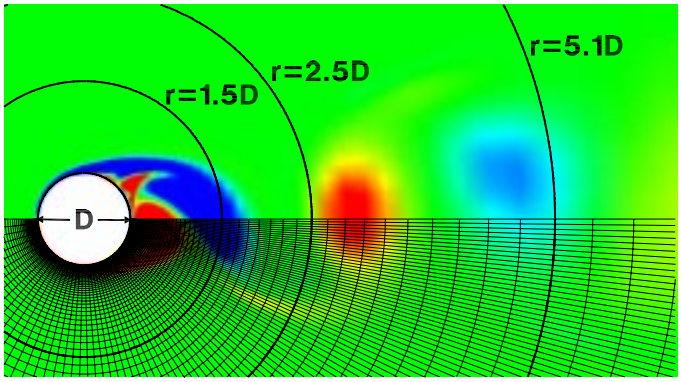

Figure 5. Vorticity field computed from CFD. FW-H integration surfaces are at $r = 0.5D$, $r = 1.5D$, $r = 2.5D$, and $r = 5.1D$

distribution on the lower portion of the figure. The positions of the FW-H integration surfaces are indicated in the upper portion of the figure. Figure 6(a) shows the computed pressure signals at the observer for the different integration surfaces using a Kirchhoff formulation, and figure 6(b) shows the the results obtained with the FW-H formulation. The use of an integration surface that cuts through the cylinder wake does not appear to adversely affect the results obtained with the FW-H formulation. However, these variations are very small compared with the results of Figure 6(a), in which the pressure computed with a standard Kirchhoff formulation for the same problem with the same integration surfaces varies wildly. This result clearly demonstrates that the FW-H should be used instead of the Kirchhoff method. Furthermore, there is very little difference in the computational effort required for the two approaches.

TRAILING-EDGE SCATTERING

Calculation methods for acoustic fields that include trailing-edge noise currently are largely empirical [18]. Singer *et al.*[17]. investigated the feasibility of directly computing the acoustic field generated by flow over a sharp trailing edge. A hybrid computational approach was taken wherein the CFL3D solver was used to accurately calculate the unsteady fluid dynamics over a relatively small region near the surface, and an acoustics code based on the Ffowcs Williams and Hawkings [10] (FW-H) equation computed the acoustic field generated by the previously calculated unsteady near flow field. To investigate edge scattering, an airfoil with vortices convecting past its trailing edge was simulated. A 2.6% thickness NACA 00 series airfoil was placed in a flow with a small, flat plate introduced perpendicular to the flow at 98% chord. In the presence of flow, vortices roll up just downstream of the flat plate, alternately near the plate's top and bottom edges.

Figure 7 shows vorticity magnitude contours in the vicinity of the trailing edge at a single time step. The circular concentrations of vorticity indicate the individual vortices that constitute the unsteady Karman vortex street downstream of the vortex-generator plate. Cases were run with Mach numbers ranging from 0.2 to 0.5 that produced regular Strouhal shedding at the plate. The frequency of the vortices convecting past the trailing edge is less distinct because the vortices shed from the vortex-generator plate often pair and interact with neighboring vortices, as shown in figure 7.

The FW-H code computed the acoustic field generated by the unsteady aerodynamic flow field. The far-field signals were obtained at several observer locations. Figure 8(a) shows spectra of the acoustic signals for several observer positions. The angular measurements are increasingly positive for counterclockwise rotations, with 0 degrees being directed downstream. The figure shows greatly reduced noise radiation directly upstream and directly downstream. Integration of each acoustic spectrum over the frequencies provides the mean square acoustic pressure. Variation of the mean square acoustic pressure as a function of Mach number is plotted in Figure 8(b). The symbols show the data, and the lines are linear least-squares fit to the logarithm of the data. For an observer at 30 degrees, the mean square pressure varies as the 5.2 power of Mach number. Accounting for the actual rms fluctuating velocity in the calculations, a theoretical scaling of $M^{5.36}$ is implied, which is in close agreement with the computationally observed scaling of $M^{5.2}$. These computations have helped to verify that the hybrid approach is valid and capable of accurately predicting fairly complicated, broadband, acoustic phenomena.

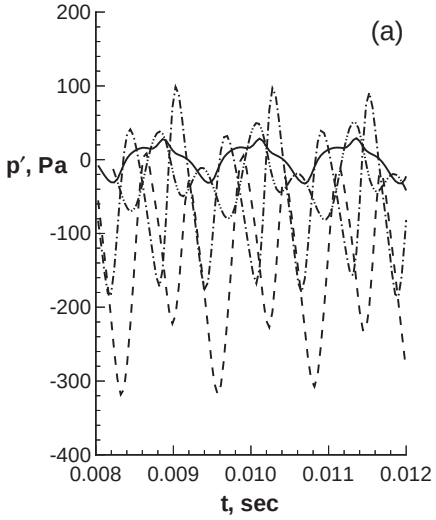

(a) Computations with Kirchhoff scheme.

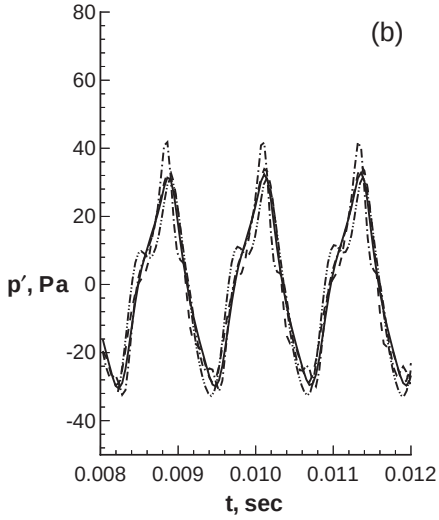

(b) Computations with FW-H scheme.

Figure 6. Acoustic signals computed for various integration surfaces that correspond to those indicated in Figure 5. Integration surfaces at ——— $r = 0.5D$, – – – – – $r = 1.5D$, —·—·— $r = 2.5D$, —··—··— $r = 5.1D$.

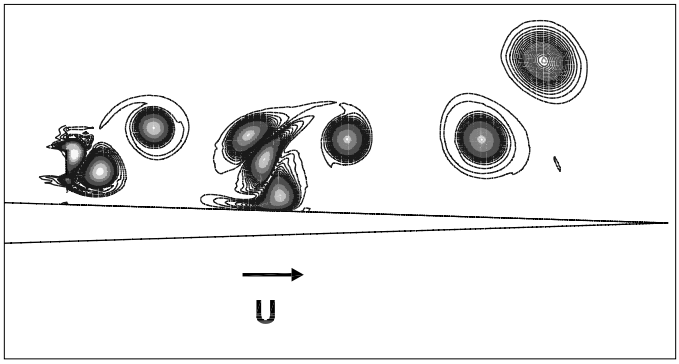

Figure 7. Instantaneous vorticity magnitude contours in vicinity of trailing edge for $M = 0.2$ case. Approximately 2% of aft portion of airfoil is shown.

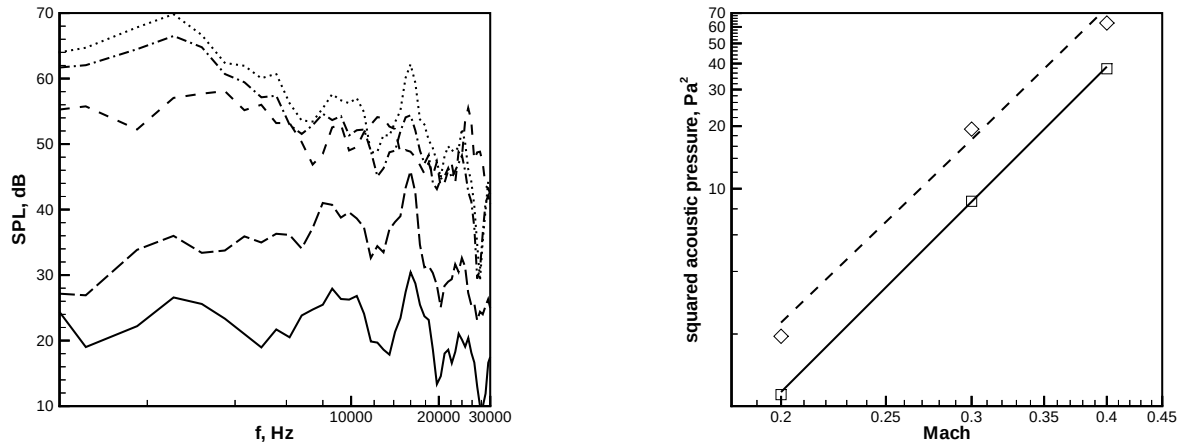

(a) (b)

Figure 8. (a) Spectra of acoustic signals (referenced to 20μPa) for observers located $10C$ from trailing edge of airfoil; on-airfoil-body integration surface used, $M = 0.2$. Observers located at: ——— 0 deg., – – – – – 45 deg., –·–·–· 90 deg., ····· 135 deg., — — — 180 deg. (b) Variation in mean square acoustic pressure versus Mach number; □ data for 30 deg., ——— least-squares fit for 30 deg., ◇ data for 45 deg., – – – – – least-squares fit for 45 deg.

HIGH-LIFT CONFIGURATION

A cooperative test involving NASA's High-Lift Program Element and NASA's Airframe Noise Team was conducted in NASA Langley Research Center's Low-Turbulence Pressure Tunnel (LTPT). The model tested in the tunnel is known as the Energy Efficient Transport (EET) model. The EET model tested includes a full-span leading-edge slat and a part-span trailing flap. To obtain acoustic data, members of Boeing Commercial Airplane Company designed and built a microphone array that was installed in the wind tunnel. The microphone array and the subsequent data processing followed techniques developed earlier at Boeing [19].

Figure 9(a) illustrates one unexpected feature of the experimental data. For a slat deflection of $\delta_s = 30$ degrees, a very large amplitude peak was observed in the acoustic spectrum in the vicinity of 50 kHz. This peak rises almost 20 dB above the signal observed for the case in which the slat is deflected 20 degrees. During the course of the experiment, efforts to eliminate the high-frequency peak by altering the overhang of the slat were largely unsuccessful. Only for cases in which the overhang became unrealistically large was a significant change in the high-frequency acoustic peak observed. Increasing the configuration's angle-of-attack from 10 to 15 degrees, reduced the amplitude of the high-frequency peak by approximately 10 dB. For some time, no consistent explanation of the observed phenomena was available.

Khorrami et al [20] provides details of unsteady, two-dimensional (2D), Reynolds-averaged Navier-Stokes (RANS) calculations designed to mimic the experimental conditions. In particular, the RANS computation was specially designed to properly incorporate and resolve the small, but finite trailing-edge thickness of the slat. Extremely small grid cells were used in the vicinity of the slat trailing edge and the time step was chosen to ensure more than 120 time steps per period of a 50 kHz signal. Slat deflections of both 30 and 20 degrees were simulated. These calculations clearly show vortex shedding from the slat trailing edge for the case with a 30 degree slat deflection. Figure 9(b) shows a snapshot of the pressure fluctuations produced in the flow field. The vortex shedding virtually disappears for the case of a 20 degree slat deflection.

Singer *et al.*[21] discuss the aeroacoustic analysis of the unsteady data. As a first approximation, the code developed by Lockard[22] for computing the 2D acoustic field from 2D CFD data was used to predict the sound field. Figure 10(a) shows computed spectra based on $1/12^{\text{th}}$ octave bins for an observer located at 270 degrees. Clearly the computed noise also has a significant peak in the spectra in the same frequency range as the experiment. This confirmed that the fluctuations from the slat vortex shedding weren't just hydrodynamic fluctuations, but also

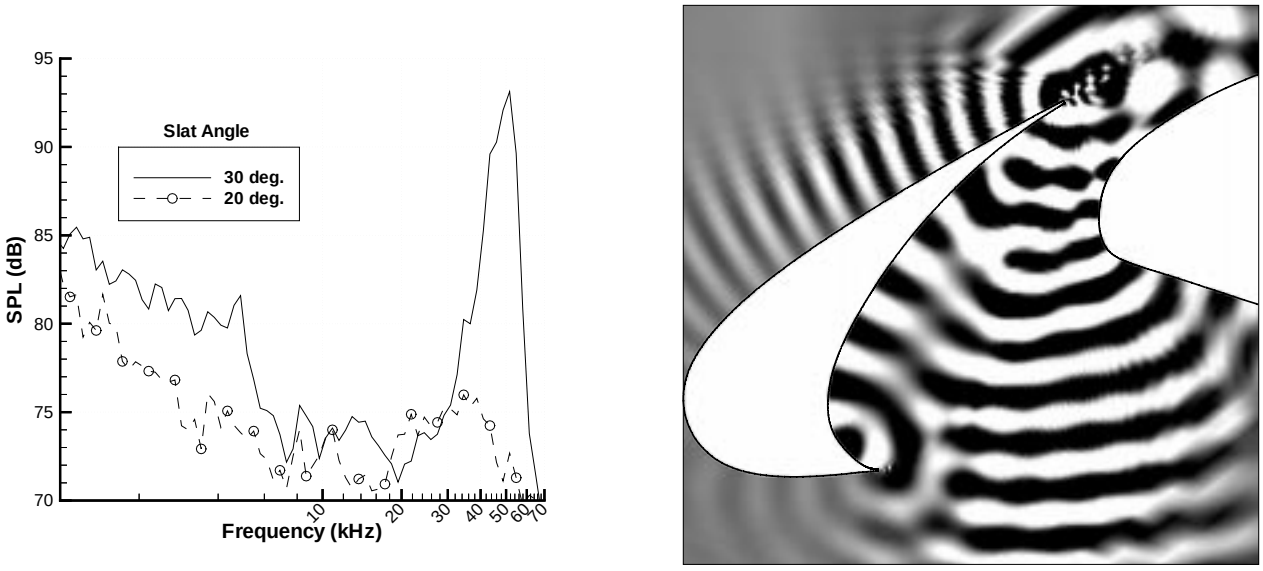

(a) (b)

Figure 9. (a) Acoustic spectrum based upon $1/12$th octave bins with array focussed on slat region. Configuration angle of attack is 10 deg., Reynolds number is 7.2 million, Mach number is 0.2. (b) Instantaneous fluctuation pressure, in vicinity of leading-edge slat, from CFD calculation. Slat deflection is 30 deg.

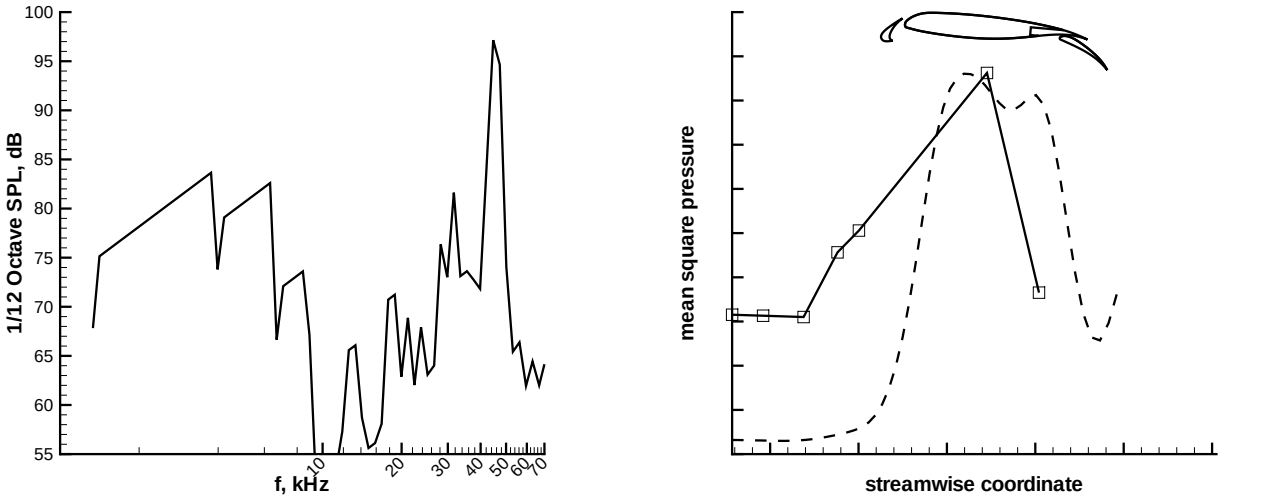

(a) (b)

Figure 10. (a) Spectra for observer positioned at 270 deg. with 30 deg. slat deflection. (b) Comparison of squared acoustic pressure at individual microphones to that predicted computationally. Microphone positions and values are shown with squares; dashed line indicates computationally predicted values.

produced noise. Although the acoustic array used in the experiment was not intended to provide any directivity information, the high-frequency acoustic signal was so loud that it overwhelmed the intrinsic wind-tunnel noise and can be identified from the spectrum of some of the individual microphones used in the acoustic array. The relative amplitudes of the mean square fluctuating pressure in a frequency range around 50 kHz from a subset of microphones having approximately the same cross-stream location are compared with computed values in Fig. 10(b). The maximum amplitude of the microphone data is scaled with the maximum amplitude of the calculation. The non-zero microphone response far-upstream is associated with the wall-pressure fluctuations of the turbulent boundary layer along the wind-tunnel ceiling. These fluctuations are not included as part of the CFD calculations. Slightly upstream of the slat leading edge, the noise level rises. The maximum amplitude occurs in the mid-chord region followed by a sharp drop in amplitude. The qualitative features of the computations agree remarkably well with the microphone data, and the directivity results aided in the redesign of the acoustic array for a subsequent wind-tunnel test.

ADVANCED TOOLS

Although great strides have been made in simulating acoustic phenomena, the costs associated with some of the calculations are clearly limiting. The unsteady RANS calculation of the 2-D slat shedding required over 100 CRAY hours. The projection for a 3-D problem is enormous. It is unlikely that advances in computer power alone will make all of the needed calculations feasible. To help bridge the gap between available resources and needed simulations, some advanced methodologies are being developed that are much more efficient and accurate than traditional methods. Two main paths are being explored. Most grids used today are still block-structured, and the macro-element technique is being developed to provide more accurate interface conditions that can be retrofitted into current codes and used in new codes with high-order finite-difference spatial operators. The other technique being developed is the discontinuous Galerkin which provides high-order on unstructured grids.

DISCONTINUOUS GALERKIN

The process of generating a block-structured mesh with the smoothness required for high-accuracy schemes is a time-consuming process often measured in weeks or months. Unstructured grids about complex geometries are more easily generated, and for this reason, methods using unstructured grids have gained favor for aerodynamic analyses. However, they have not been utilized for acoustics problems because the methods are generally low-order and incapable of propagating waves without unacceptable levels of dissipation and dispersion. Attempts to extend finite-difference and finite-volume methods for unstructured grids to high-order by increasing the stencil size have introduced storage and robustness problems.

The discontinuous Galerkin method[23, 24] is a compact finite-element projection method that provides a practical framework for the development of a high-order method using unstructured grids. Higher-order accuracy is obtained by representing the solution as a high-degree polynomial whose time evolution is governed by a local Galerkin projection. This approach results in a compact and robust method whose accuracy is insensitive to mesh smoothness. The traditional implementation of the discontinuous Galerkin uses quadrature for the evaluation of the integral projections and is prohibitively expensive. Atkins and Shu[25] introduced the quadrature-free formulation in which the integrals are evaluated a-priori and exactly for a similarity element. The approach has been demonstrated to possess the accuracy required for acoustics even in cases where the grid is not smooth. Other issues such as boundary conditions and the treatment of non-linear fluxes have also been studied in earlier work[26, 27].

A major advantage of the discontinuous Galerkin method is that its compact form readily permits a non-heterogeneous treatment of a problem. That is, the shape of elements used, the degree of approximation, even the choice of governing equations, can be allowed to vary from element to element with no loss of rigor in the method. To take advantage of this flexibility, an object-oriented C++ computer program that implements the discontinuous Galerkin method has been development and validated. However, many of the applications have involved benchmark problems for aeroacoustics[5] with relatively simple two-dimensional geometries and linearized equations with uniform mean flows. Recent work has been aimed at adding and validating additionally capability that is essential to the aeroacoustic analysis of large complex configurations.

Current applications of the method involve three-dimensional problems, the treatment of nonuniform mean flows, viscous flows, and the efficient use of parallel computing platforms. With these new capabilities, this tool will enable rapid aeroacoustic analyses of realistic aircraft configurations. When coupled with currently available grid generators and large parallel computers, the entire process of mesh generation, problem setup, and calculation can be performed

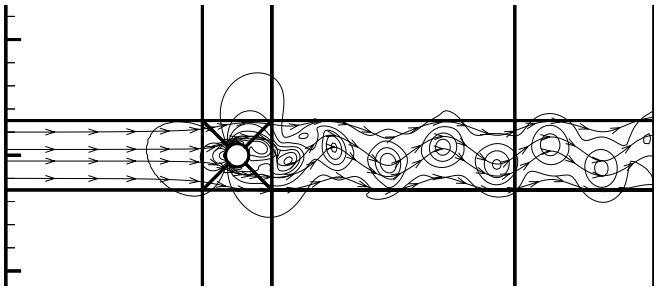

Figure 11. Density contours and streamlines for flow over a circular cylinder. The Mach number is 0.4 and the Reynolds number is 150. Dark lines represent macro-element boundaries.

rapidly.

MACRO-ELEMENT FINITE-DIFFERENCE

The most common approach used to handle complex geometries in CFD is the use of block-structured grids. There are many different varieties including one-to-one point matching, arbitrary patching, and overset zonal boundaries, but all require some sort of method to transfer information between the different blocks. Most codes rely on low-order interpolation formulas that can produce small but obvious artificial discontinuities in the flow variables across the boundaries. The problem is usually much more severe for unsteady problems when the grid is not sufficiently fine. Furthermore, interface conditions generally do not have suitable error properties and contribute to the nearly universal problem of codes not converging to design accuracy for realistic problems. Still, there has been a great deal of research into the proper methodologies for solving discrete equations efficiently on structured grids, and structured grids continue to be preferred for boundary layer flows.

In addition to the standard problems in CFD, most practitioners involved in unsteady computations, including aeroacoustics, prefer to use structured meshes. At several workshops[4, 5] on computational aeroacoustics, high-order, finite-difference methods have been shown to be much more efficient at minimizing dissipation and dispersion in propagating acoustic waves than traditional methods with many grid points. However, finite-difference methods perform best on smooth, structured grids which are often difficult to generate. Furthermore, high-order methods often suffer from robustness and stability problems stemming from non-smooth meshes and discontinuous flows. Blocking allows structured grids to be used around complex geometries, and makes it somewhat easier to make the grids smooth. However, standard patching techniques are wholly unsuited for high-order methods, especially for unsteady flows. Not only do they not provide adequate accuracy, they are often unstable. High-order methods would also benefit from interface conditions that could be used to break up larger domains so that subdomains could be run on different nodes of a parallel computer. With the continued advancements in parallel computers comprised of many scalar processors, this is becoming a very important issue.

In a coordinated effort, Carpenter *et al.*[28, 29] have developed high-order patching conditions with both order and stability proofs for high-order methods. The individual blocks are referred to as macro-elements. The only requirement for the grid is that the interface be point matched, or C_0, but the derivatives may be discontinuous. Although not completely general, it does provide some significant flexibility in grid generation and is useful for splitting up a domain for a parallel computation. Conditions for fourth- and sixth-order explicit as well as fourth-order compact have been developed. Figure 11 shows density contours and streamlines around a circular cylinder with a grid partitioned into macro-elements. The Mach number is 0.4 and the Reynolds number is 150 which produces strong vortex shedding. Notice that there are nearly triangular shaped elements in the vicinity of the cylinder, yet there is no apparent distortion to the contours or streamlines. The macro-element conditions are general enough that they could even be used as interface conditions for an unstructured grid.

LOW-STORAGE RUNGE-KUTTA

Although most of the previous discussion has focused on the spatial operators, it is just as important to maintain temporal accuracy in unsteady problems. Explicit Runge-Kutta time-stepping provides a simple way to obtain high-accuracy in time, but most of the classical formulas have high memory requirements to store many previous solutions or residuals. Kennedy *et al.*[30] have developed fourth- and fifth-order explicit Runge-Kutta formulas that

only require $2N$ storage for N unknowns. This can be a substantial savings in memory, and can also be very beneficial in the run time on cache-based computers which are often limited by memory access. Furthermore, some of the new Runge-Kutta methods have embedded lower-order formulas that allow for automated time-stepping by using the solutions from the two orders to determine if there is too much error and the time step needs to be decreased.

A difficulty with explicit time stepping for unsteady problems is that the time step must be chosen to keep the smallest cell in the entire grid stable. In boundary layer flows with strong clustering towards walls, this can result in a time-step orders of magnitude smaller than what is needed for temporal accuracy. Research is ongoing into different implicit methods that can be used in regions where the grid spacing is extremely small.

SUMMARY

Despite the simplifications used in the examples, the cost of performing many of the acoustic calculations was still very high. Just obtaining a highly resolved mean flow for a high-lift flap system required 50 CRAY C-90 hours, and an unsteady RANS of a two-dimensional slat problem required over 100 hours. Nonetheless, some significant insight has been gained by applying currently available computational techniques to problems of interest. Typically, the calculations concentrated on resolving certain frequency ranges rather than trying to solve for all of the scales simultaneously. Because many important noise sources are narrow band, this approach is appropriate. The noise generated from vortex-shedding at a slat trailing edge is a good example in which this approach was taken, and a previously unknown noise source was identified. There remain many problems that cannot be solved today, and some of the efforts at NASA Langley to develop advanced tools that will enable the next generation of acoustic simulations have been highlighted.

ACKNOWLEDGMENTS

The author would like to thank the members of the Computational Modeling and Simulation Branch at NASA Langley Research Center for their significant contributions to this paper.

REFERENCES

1. W. R. WATSON, M. G. JONES, S. E. TANNER and T. L. PARROTT 1996 *AIAA Journal* **34**(3), 548–554. Validation of a numerical method for extracting liner impedance.

2. P. J. MORRIS, Q. WANG, L. N. LONG and D. P. LOCKARD 1997 *AIAA Paper No.* 97-1598. Numerical predictions of high-speed jet noise.

3. J. C. HARDIN and D. S. POPE 1994 *Theoretical and Computational Physics* **6**(5-6). An acoustic/viscous splitting technique for computational aeroacoustics.

4. J. C. Hardin and M. Y. Hussaini, editors 1993 *Computational Aeroacoustics*. Springer-Verlag. (Presentations at the Workshop on Computational Aeroacoustics sponsored by ICASE and the acoustics division of NASA LaRC on April 6-9.)

5. C. K. W. Tam and J. C. Hardin, editors 1997 *Second Computational Aeroacoustics (CAA) Workshop on Benchmark Problems*. NASA CP-3352. (Proceedings of a workshop sponsored by NASA and Florida State University in Tallahassee, Florida on Nov. 4-5, 1996.)

6. C. RUMSEY, R. BIEDRON and J. THOMAS 1997 *TM* 112861. NASA. (presented at the Godonov's Method for Gas Dynamics Symposium, Ann Arbor, MI.) CFL3D: Its history and some recent applications.

7. S. L. KRIST, R. T. BIEDRON and C. RUMSEY 1997. NASA Langley Research Center, Aerodynamic and Acoustic Methods Branch. *CFL3D User's Manual (Version 5)*.

8. C. L. RUMSEY, M. D. SANETRIK, R. T. BIEDRON, N. D. MELSON and E. B. PARLETTE 1996 *Computers and Fluids* **25**(2), 217–236. Efficiency and accuracy of time-accurate turbulent Navier-Stokes computations.

9. M. J. LIGHTHILL 1952 *Proceedings of the Royal Society* **A221**, 564–587. On sound generated aerodynamically, I: general theory.

10. J. E. FFOWCS WILLIAMS and D. L. HAWKINGS 1969 *Philosophical Transactions of the Royal Society* **A264**(1151), 321–342. Sound generated by turbulence and surfaces in arbitrary motion.

11. K. S. BRENTNER and F. FARASSAT 1998 *AIAA Journal* **36**(8), 1379–1386. An analytical comparison of the acoustic analogy and kirchhoff formulation for moving surfaces.

12. F. FARASSAT and G. P. SUCCI 19883 *Vertica* **7**(4), 309–320. The prediction of helicopter discrete frequency noise.

13. K. S. BRENTER 1986. NASA Langley Research Center. (NASA TM 87721.), *Prediction of Helicopter Discrete Frequency Rotor Noise – A Computer Program Incorporating Realistic Blade Motions and Advanced Formulation*

14. K. S. BRENTNER and F. FARASSAT 1994 *Journal of Sound and Vibration* **170**(1), 79–96. Helicopter noise prediction: The current status and future direction.

15. C. L. RUMSEY, R. BIEDRON, F. FARASSAT and P. L. SPENCE 1998 *Journal of Sound and Vibration* **213**(4), 643–664. Ducted-fan engine acoustic predictions using a Navier-Stokes code.

16. C. L. STREETT 1998 *AIAA Paper No.* 98-2226. Numerical simulation of a flap-edge flowfield.

17. B. A. SINGER, K. S. BRENTNER, D. L. LOCKARD and G. M. LILLEY 1999 *AIAA Paper No.* 99-0231. Simulation of acoustic scattering from a trailing edge.

18. S. WAGNER, R. BAREISS and G. GUIDATI 1996 *Wind Turbine Noise*. New York: Springer.

19. J. R. UNDERBRINK and R. P. DOUGHERTY 1996 *NOISECON 96*. Array design for non-intrusive measurments of noise sources.

20. M. R. KHORRAMI, M. E. BERKMAN, M. CHOUDHARI, B. A. SINGER, D. L. LOCKARD and K. S. BRENTNER 1999 *AIAA Paper No.* 99-1805. Unsteady flow computations of a slat with a blunt trailing edge.

21. B. A. SINGER, D. L. LOCKARD, K. S. BRENTNER, M. R. KHORRAMI, M. E. BERKMAN and M. CHOUDHARI 1999 *AIAA Paper No.* 99-1802. Computational acoustic analysis of slat trailing-edge flow.

22. D. P. LOCKARD. (to appear in *journal of sound and vibration*.) An efficient, two-dimensional implementation of the Ffowcs Williams and Hawkings equation.

23. C. JOHNSON and J. PITKARATA 1986 *Mathematics of Computation* **46**(176), 1–26. An analysis of the discontinuous Galerkin method for a scalar hyperbolic equation.

24. B. COCKBURN and C.-W. SHU 1998 *SIAM Journal of Numerical Analysis* **35**, 2440–2463. The local discontinuous Galerkin method for time-dependent convection-diffusion systems.

25. H. L. ATKINS and C. W. SHU 1997 *AIAA Journal* **36**(5), 775–782. Quadrature-free implementation of discontinuous Galerkin method for hyperbolic equations.

26. H. L. ATKINS 1997. AIAA Paper-97-1581. (Third Joint CEAS/AIAA Aeroacoustics Conference, May 12-14.) Continued development of the discontinuous Galerkin method for computational aeroacoustic applications.

27. H. L. ATKINS 1997. AIAA Paper 97-2032. (13th AIAA computational fluid dynamics conference, Snowmass Village, Colorado, June 29-July 2.) Local analysis of shock capturing using discontinuous Galerkin methodology.

28. M. H. CARPENTER, J. NORDSTROM and D. GOTTLEIB 1999 *Journal of Computational Physics* **148**, 341–365. A stable and conservative interface treatment of arbitrary spatial accuracy.

29. M. H. CARPENTER and J. NORDSTROM 1999 *Journal of Computational Physics* **148**, 621–645. Boundary and interface conditions for high-order finite-difference methods applied to the Euler and Navier-Stokes equations.

30. C. A. KENNEDY, M. H. CARPENTER and R. LEWIS. (to appear in *applied numerical mathematics*.) Low-storage explicit Runge-Kutta schemes for the compressible Navier-Stokes equations.